

Towards Integrated Molecular Electronic Devices: Characterization of Molecular Layer Integrity During Fabrication Processes

Amr M. Mahmoud, Adam Johan Bergren,* Nikola Pekas, and Richard L. McCreery

Reproducible carbon/molecule/Cu molecular junctions are made with high yield using diazonium reduction of aromatic molecules on carbon with direct evaporation of Cu as a top contact. This report investigates the stability of these devices in response to fabrication steps. Raman spectroscopy through a transparent support shows that direct deposition of Au or Cu causes little change in molecular layer structure, while Ti and Pt deposition cause significant damage to the molecules. AFM, Raman, and XPS examination of Au, Cu, and Ti devices after removal of deposited metal confirm that Cu and Au have minimal effects on molecular structure. However, the molecular layer is rougher after Au deposition, probably due to partial penetration of Au atoms into the molecular layer. Completed carbon/molecule/Cu devices can be heated to 250 °C without significant changes in electronic behaviour while nitroazobenzene molecular layers on carbon were unaffected by photolithography or by 5 min at 400 °C in vacuum. Completed devices could be sealed with parylene-N, stabilizing them to aqueous etching solution. The stability of carbon/molecule/Cu junctions is due, in part, to the strong carbon-carbon bonding and aggressive nature of diazonium surface modification. The results significantly expand the range of processing variables compatible with molecular electronic junctions.

which investigates charge transport through molecules that are configured as circuit components, attempts to use molecules or molecular layers as circuit components. In addition to serving as a guide for understanding the electronic behaviour of molecules, there is also the possibility of using the electronic properties of the molecules themselves in new and interesting ways. Thus, the development of molecular electronic devices may not only enable the continuation of Moore's law, but may also result in enhancements in performance or functions that are not possible with current semiconductor technology.

For any embodiment of molecular electronics to serve a real-world function, integration of molecular and semiconductor devices is essential. However, conventional semiconductor processing often involves the use of harsh fabrication conditions that are acceptable for inorganic materials, but pose potential problems for the "soft" organic molecules used in molecular devices. Thus,

any practical molecular electronics platform must be amenable to the necessary procedures required to produce a fully integrated electronic chip. To this end, there are two possibilities: 1) integration of molecular devices into a hybrid circuit composed of both the molecular and traditional components, and 2) production of a fully molecular circuit in a massively parallel fashion. In either case, there are numerous fundamental issues that require investigation. In the case of a hybrid chip consisting of both traditional and molecular devices, it is critical to ensure that the molecular device can withstand the conditions required for integration.

Various platforms have been developed to study the electrical characteristics and charge transport mechanism in molecular junctions.^[9–13] In many cases, these studies have greatly contributed to our understanding of charge transport in molecular devices, but are currently limited to research labs. For example, liquid metal top contacts^[9,14–16] and STM^[10] or AFM tips^[13] have been used to avoid the harsh conditions associated with vapour deposition steps required for metallization. These techniques have enabled the construction of molecular junctions using labile molecular self-assemblies, but are not readily adaptable to massively parallel fabrication. In order to overcome these limitations, a method using conducting polymer top contacts

1. Introduction

Integration of electronic components into miniaturized platforms that can accomplish targeted functions has led to the ubiquitous implementation of integrated circuits (ICs). The low cost, high device density, and ability to package microchips and incorporate them into durable products has led to a thriving semiconductor industry with sales exceeding \$225 billion (USD) in 2009.^[1] This level of success relies largely on the ability to fabricate the electronic circuits in a highly parallel fashion. The developing field of molecular electronics,^[2–8]

A. M. Mahmoud, Prof. R. L. McCreery
University of Alberta
Edmonton, Alberta, Canada T6G 2G2
Dr. N. Pekas, Prof. R. L. McCreery
National Institute for Nanotechnology
Edmonton, Alberta, Canada T6G 2M9
Dr. A. J. Bergren
National Institute for Nanotechnology
Edmonton, Alberta, Canada T6G 2M9
E-mail: Adam.Bergren@nrc.ca

DOI: 10.1002/adfm.201002496

that is capable of producing devices based on Au/thiol self assembled monolayers (SAM) on a massively parallel scale (i.e., 20 000 molecular junctions on one wafer) has been demonstrated.^[11] However, SAM-based devices have limited thermal stability. In two different studies, the upper limit of the temperature process window of SAM-based molecular junctions on gold and Si has been determined to be 50 and 100 °C, respectively.^[17,18] Another critical requirement is making contact with the molecular layers without inducing structural damage. Various techniques for avoiding damage to SAM-based devices have been published^[19,20] and numerous reports exist that discuss post-deposition damage to molecular layers.^[21–24]

We have pursued an alternative approach to using self-assembled monolayers in junction fabrication that relies on covalent modification of carbon electrodes through the electrochemical reduction of aryl diazonium salts.^[12,15,25–29] As detailed in the experimental section, carbon electrodes comprise pyrolyzed photoresist film (PPF), with rms (root mean square) surface roughness of about 0.5 nm. There are several advantages to this method: the layers are anchored by a carbon–carbon bond that is much stronger (3.5 eV) than Au–S linkages (1.9 eV),^[4] the thickness can be controlled in the 1–5 nm range by changing the conditions during the electrochemical reduction step,^[26,30–32] and a variety of aromatic structures can be accommodated.^[12] To complete the circuit, metallic copper^[12,25,29,33] is deposited as a top contact by direct electron-beam evaporation to form a cross-junction. These devices display yields exceeding 90% and have excellent reproducibility. In addition, they survive at least 10^9 electric potential cycles in ambient air,^[26] and they are scalable (i.e., the current scales with junction dimension from at least $400\ \mu\text{m} \times 400\ \mu\text{m}$ to $16\ \mu\text{m} \times 16\ \mu\text{m}$)^[34].

In this paper, we describe analytical techniques to investigate the stability of diazonium-derived molecular layers on carbon undergoing various fabrication procedures, including metal deposition, lithography, etching, and temperature excursions. Several top contact metals were deposited using direct electron beam evaporation, and the integrity of the molecular layer was investigated by performing spectroscopic characterization through a partially transparent support. In addition, the molecular layer was examined with Raman spectroscopy and X-ray photoelectron spectroscopy (XPS) after removal of the top contact by etching with appropriate etchants for each metal used. Using similar procedures, the layer integrity was investigated after subjecting the samples to conditions that are commonly encountered in semiconductor integration such as UV lithography and packaging procedures and it is shown that the electronic properties of the molecular devices are unchanged by packaging with parylene. Finally, the thermal stability of finished molecular junctions was investigated.

2. Results and Discussion

2.1. Electrical Characterization Using Different Top Contacts

Figure 1 shows current density–voltage (J – V) curves for PPF/molecule junctions made using 4-nitroazobenzene (NAB)

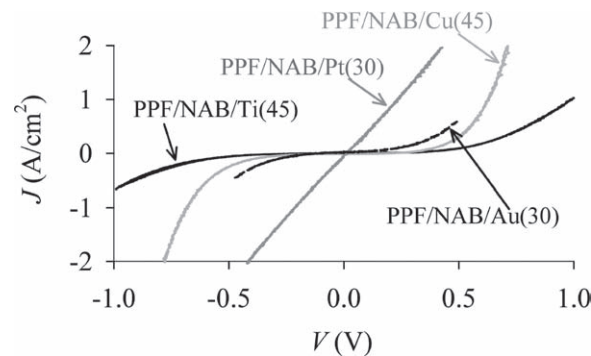


Figure 1. J – V curves of Si/SiO₂/PPF/NAB/metal junctions for four different top metals contact (Cu, Au, Ti, and Pt). Scan rate 1000 V/s.

diazonium salt and four different top metal contacts: Cu, Au, Ti, and Pt. There are significant differences between junctions made with different metals. First, when Pt is used as the top contact, the J – V response is linear and behaves similar to a short circuit with direct metal to PPF contact, while all of the other curves show some degree of non-linearity. Second, as shown in Figures S1 and S2 in the Supporting Information, there are significant differences in the reproducibility of the junctions made using Cu and Au. The electrical behaviour of Cu devices has been shown in the past to depend on molecular structure and molecular layer thickness.^[12,25,26] In addition, reproducibility is typically very high and yields exceed 90%.^[12,26,34] The present results are comparable to previous reports in terms of curve shape and magnitude, yield, and reproducibility (the relative standard deviation, or rsd, for the current density at 0.5 V for 12 PPF/NAB/Cu junctions is 12%). Furthermore these results are similar to those obtained with “soft” deposition through surface diffusion of copper onto an NAB molecular layer.^[35] However, the electrical behaviour of PPF/NAB/Au junctions is less reproducible than that of the Cu devices (Figure S2 shows that the rsd of the current density at 0.5 V is ~55% for Au devices). These results may be attributed to partial penetration of Au into the NAB molecular layer as discussed below. Third, Ti metal is a highly reactive species that can react with residual gases in the evaporation chamber, forming, for example, titanium oxides^[29,36,37] which are less conductive than Ti metal. This leads to the junction conductance being at least partially controlled by the oxidized Ti, complicating the analysis. In addition, the highly reactive Ti metal can undergo reactions with the molecular layer itself, possibly altering or destroying it.^[21,23,38] In order to address these various possibilities, we have determined the thermal stability of NAB chemisorbed on PPF, determined the temperature rise at the location of the substrate in the vacuum chamber during deposition, used spectroscopic characterization through transparent supports to track any structural changes in the molecular layer during fabrication processes, and used XPS and AFM to characterize structural and morphological changes to the molecular layer after removal of the top contact metals.

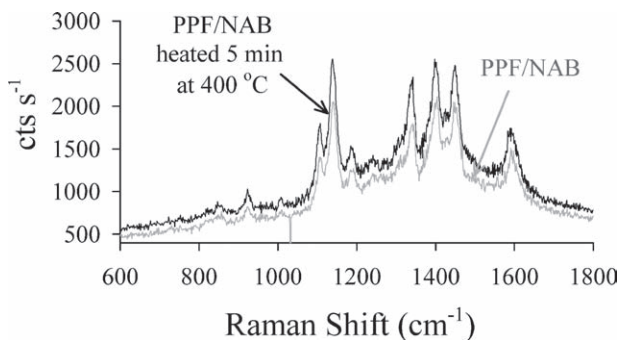


Figure 2. Raman Spectra for PPF/NAB before (gray curve), and after (black curve) heating for 5 min to 400 °C in a $\sim 2 \times 10^{-6}$ torr vacuum.

2.2. Temperature Stability of NAB on PPF

In order to determine the thermal stability of a diazonium-derived molecular layer on carbon, a sample of PPF/NAB was heated to 400 °C in vacuum ($\sim 2 \times 10^{-6}$ torr) for 5 min. **Figure 2** shows Raman spectra for this sample before and after heating, and Table S1 in the supporting information lists the relative peak intensities. The absence of a significant change in absolute or relative Raman intensities indicates that no observable structural change occurred at 400 °C for 5 min in vacuum. This indicates that any procedure that results in a temperature rise of 400 °C or less in vacuum is not expected to cause thermally-induced damage to an NAB layer bonded to PPF. While stability may vary with molecular structure, the current results indicate that the surface C–C bond of diazonium-derived adlayers on PPF is stable to >400 °C in vacuum. However, we note that the NAB film is less stable in an Argon atmosphere than in vacuum, with changes in the Raman spectrum observable above 250 °C (Figure S-3). The structural changes of the NAB film in Ar are presumably due to Ar collisions with the NAB surface or reactions with residual oxygen in the Ar atmosphere. These results are consistent with those of Toupin and Belanger,^[39] who reported thermal stability of similar molecular layers to 250–500 °C, depending on atmosphere and exposure time.

2.3. Spectroscopic Characterization of Molecular Layer Integrity

We have previously applied “backside” Raman spectroscopy to investigate the integrity of an NAB molecular layer on an ultrathin titanium primer layer supported on quartz after deposition of Au and Ag metals.^[40] Here we apply the same method, but use partially transparent PPF (OTPPF) on quartz to more closely replicate conditions in molecular junctions. This approach enables a direct correlation between Raman characterization and electrical measurements, since the latter are carried out using thick PPF films as the substrate. **Figure 3** shows the Raman spectra of Q/OTPPF/NAB initially (gray curves) and after deposition (black curves) of four different top metal contacts: Cu (A), Au (B), Ti (C) and Pt (D), and intensity changes are tabulated in Table S2 of “supporting information.” Peak assignments and vibrational analysis of NAB bonded to

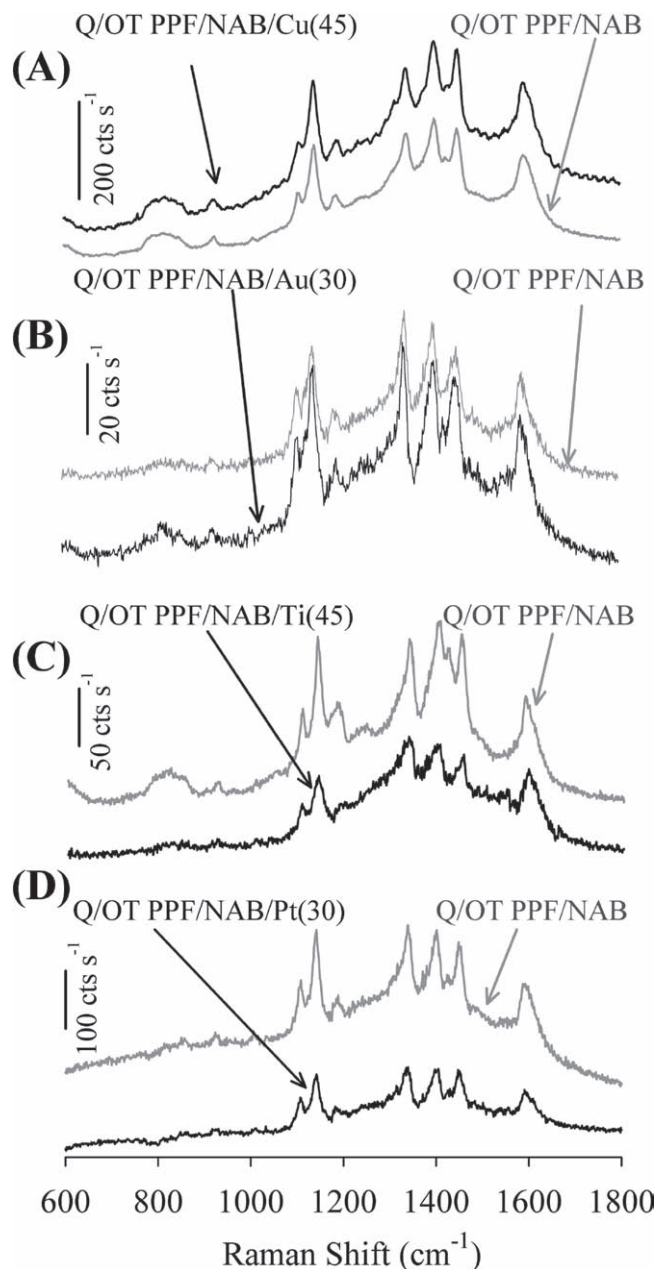


Figure 3. “Backside” Raman Spectra of Q/OTPPF/NAB before (gray curves) and after (black curves) deposition of the indicated thickness (in nm) of A) Cu, B) Au, C) Ti and D) Pt.

carbon surfaces has been reported previously.^[36,41,42] Analysis of Figure 3 shows that deposition of both Cu and Au has minimal effects on the Raman spectrum for NAB. Although the change in optical geometry accompanying metal deposition makes intensity comparisons semi-quantitative, it is clear that Ti and Pt have a much greater effect on the NAB spectrum than Au and Cu. In addition, Raman spectra obtained for Au, Cu, and Ti after removal of the top contact metal by etching show minor changes in the case of Au and Cu compared to the non-metallized samples, but nearly complete loss of the spectrum for Ti (Figure S4 in supporting information and discussion

below). This result indicates that some structural changes and/or a decrease in the surface concentration of NAB molecules occurred during Ti and Pt deposition.

In the case of Ti, the effect observed in Figure 3 is larger than that reported previously,^[37] due to the significantly greater thickness of Ti in the current case (45 nm compared to 1–3 nm). In any case, it is clear that Ti metal must be used with caution, as it is possible that this reactive metal can cause damage to the molecular layer.^[21,23] The larger effect of Pt on the NAB layer compared to Cu and Au likely results from the heat released during condensation of the metal on the molecular layer surface. The Pt heat of evaporation ($\Delta H_{\text{vap}} 509.9 \text{ kJ mol}^{-1} = 5.28 \text{ eV}$) is higher than that for Au ($\Delta H_{\text{vap}} 341.9 \text{ kJ mol}^{-1} = 3.46 \text{ eV}$) and Cu ($\Delta H_{\text{vap}} 304.3 \text{ kJ mol}^{-1} = 3.15 \text{ eV}$).^[43] Thus, it is possible that Pt deposition on the molecular layer results in significantly greater local heating from Pt condensation compared to Cu and Au. Recalling that PPF/NAB/Pt junctions behave as short circuits (i.e., a linear J - V curve is observed without any signature from the molecule), the results in Figure 3 indicate that Pt deposition causes enough damage to result in direct PPF-Pt contact. Although the spectra for Au and Cu show less changes overall, the ratio of peak intensities at 1400 to 1450 cm^{-1} before and after metal deposition is changes most for Au and Cu and is constant for Ti and Pt. This might imply that all of the Raman peaks decrease in intensity uniformly for Ti and Pt due to widespread destruction of the molecular layer. In addition, the small change in this ratio for Au and Cu may indicate either a small perturbation of the structure of the molecular layer by deposition of these metals or a specific interaction with them (e.g., chemical reduction^[37]). In any case, it is clear the Raman spectra show significantly more changes for deposition of Ti and Pt relative to Au or Cu. To provide further insight into the mechanism for damage to the molecular layer, we have obtained Raman and XPS spectra of molecular layers after removal of the metal top contact using etchants appropriate for each metal.

Figure 4 shows high-resolution XPS spectra of the N_{1s} region for samples of PPF/NAB obtained before metal deposition (solid gray curves) and after removing the metal with a chemical etch (black curves). Also shown are the spectra obtained after PPF/NAB (non-metallized) is exposed to the wet etching procedure for each case (dashed black curves). These spectra ensure that any changes detected upon metal etching originate from metal deposition and are not artefacts of the wet etching process. Note that spectra are shown for Au, Cu, and Ti, as etching of these metals is straightforward. However, in the case of Pt metal, the etching procedure is considerably more aggressive and was not attempted. In each of the three cases where metal was removed by etching, no residual metal was detected by XPS (data not shown). The N_{1s} region of the NAB spectrum is composed of two peaks: one centered at 400.2 eV, corresponding to the azo group, and a second peak at 405.9 eV, corresponding to the nitro group. The similarity of the gray and dashed black spectra in Figure 4 indicates that wet etching processes (with FeCl_3 , KI/I_2 and HF) by themselves affect neither the ratio nor the intensity of the two N_{1s} peaks. This result also indicates good chemical stability of the covalently bonded layer, as reported previously.^[44] Table 1 presents a summary of the XPS atomic N/C ratio for both the azo (400.2 eV) and nitro (405.9 eV) peaks before and after metal etching. Direct evaporation of Cu

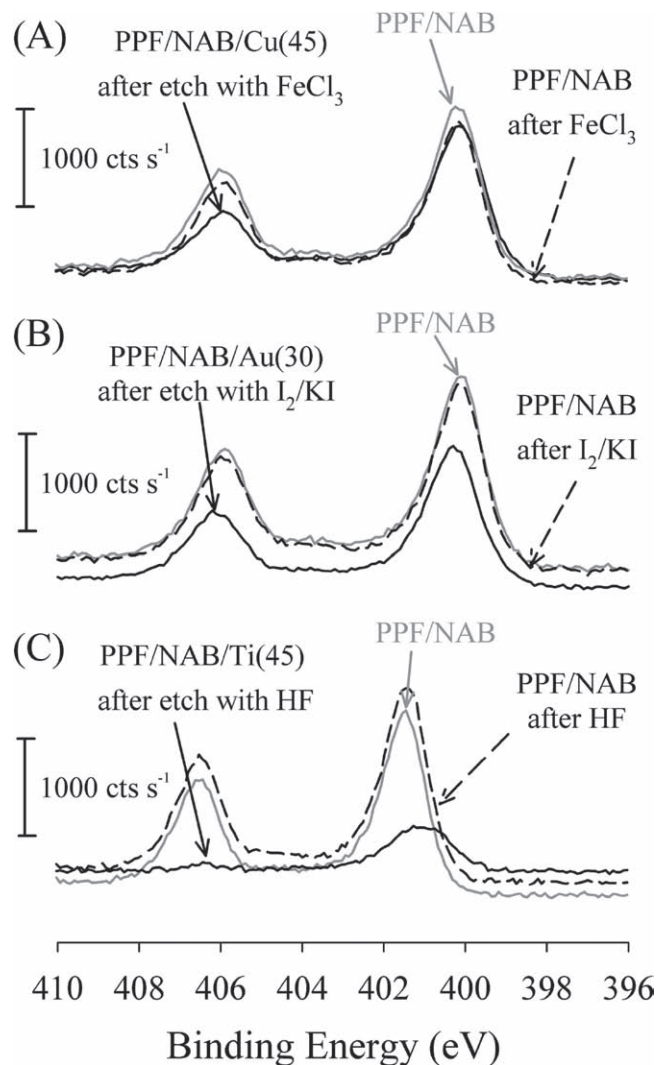


Figure 4. High-resolution XPS spectra of the N_{1s} region for three samples of $\text{Si/SiO}_2/\text{PPF/NAB}$. The gray curves were obtained before treatment, the black curves after metal deposition and etching, and the dashed black curves after immersion of $\text{Si/SiO}_2/\text{PPF/NAB}$ samples in etchant solution without metal deposition. A) Cu (45 nm) and etchant FeCl_3 ; B) Au (30 nm) and etchant KI/I_2 ; C) Ti (45 nm) and etchant HF.

(45 nm) onto NAB (black curve in Figure 4A) does not measurably impact the azo group of NAB molecules (the $N_{400.2}/C$ ratio is 0.10 before and 0.11 after). However, the nitro peak (405.9 eV) undergoes a decrease (the $N_{405.9}/C$ ratio is 0.058

Table 1. XPS atomic ratios of N_{1s} of NAB molecular layer on PPF substrate initially and after deposition and etching of the metal top contact.

Metal	N/C of N 400.2 eV (azo)		N/C of N 405.9 eV (nitro)	
	Initially	After metal etch	Initially	After metal etch
Cu	0.10	0.11	0.058	0.033
Au	0.11	0.10	0.057	0.045
Ti	0.12	0.03	0.068	0.002

before and 0.033 after). This reduction in the peak ratio may be attributed to either reduction of the nitro group by Cu deposition^[36,42] or loss of peripheral nitro groups. For the case of Au deposition on PPF/NAB, there is minimal change in the N/C ratio or the relative intensities of the 400 and 406 eV N_{1s} peaks. Finally, Figure 4C shows the effect of Ti deposition on NAB. In this case, comparison of the spectrum after removal the Ti overlayer to that before deposition of Ti shows that the peak associated with the nitro group is dramatically affected. The N_{405,9}/C ratio decreases from 0.068 to 0.002, indicating nearly complete loss of the nitro group. In addition, the N_{400,2}/C ratio diminished by more than 75%. Although a Ti–N bond appearing at 397 eV has been reported after deposition of Ti onto PPF/NAB sample,^[36] in the current case, the HF etch removed all titanium from the surface (no Ti XPS peaks were observed). As discussed above, Raman spectra were also obtained after removal of top contact metals (Figure S4 in the supporting information) to ensure optical artefacts with the metal overlayer present do not affect the spectra. It is striking to note that the molecular signature of NAB is absent from the surface after etching Ti, consistent with XPS data indicating the near total loss of the NAB structure. Combining the Raman and XPS results on the etched surfaces, we conclude that direct electron-beam deposition of Cu and Au does not cause destruction of the NAB film, while deposition of Pt and Ti causes substantial structural changes. In the case of Ti, it is likely that the reactivity of the Ti metal during evaporation results in damage through titanium carbide (and possibly other) bond formation. When the Ti metal is etched, the molecule is removed from the surface along with any Ti metal. For the case of Pt metal, it is likely that the heat released during condensation of the metal on the molecular layer results in local heating that is sufficient to disrupt some of the chemical bonds present, but does not entirely remove the layer from the surface.

2.3. Evaluation of Sample Morphology

Although Au and Cu deposition caused minimal changes in Raman and XPS spectra of the NAB layer, it is possible that their deposition causes morphological changes. We investigated the film morphology with AFM after etching of Cu and Au. PPF/NAB surfaces before metal deposition were smooth, with no visual variations across a several μm^2 area and an rms roughness value similar to underivatized PPF (~ 0.46 nm, see Figure S5A,B in supporting information). Figure 5 shows AFM images of PPF/NAB after deposition and etching of 45 nm of Cu or Au, using the same parameters as those for junction preparation. Figure 5A shows that deposition and removal of Cu metal had minor effects on the appearance of the AFM image, and an insignificant change in surface roughness to 0.47 ± 0.03 nm. However, after deposition and etching of Au, the rms roughness of the molecular layer more than doubled to 1.12 ± 0.37 nm, and the AFM image was noticeably different (Figure 5B). A control experiment in which an uncoated PPF/NAB sample was subjected to the etchant used to remove Au showed no changes in roughness or morphology (see Figure S6 in the supporting information). Together with the higher currents observed for PPF/NAB/Au junctions compared to PPF/NAB/

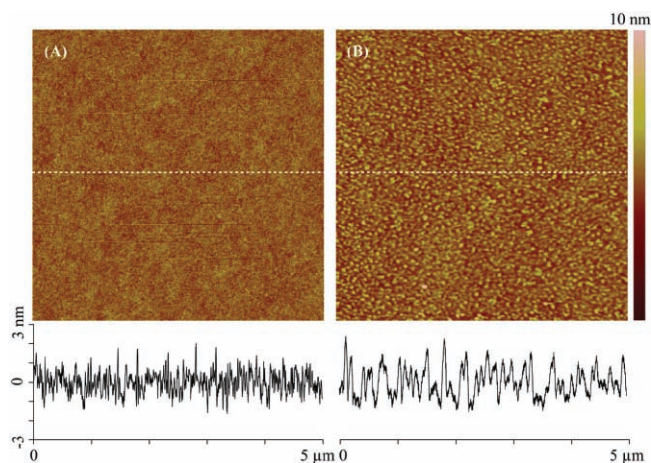


Figure 5. AFM scan of PPF/NAB surface with corresponding line scans after etching the top metal; in (A), the top metal was Cu, while in (B), the top metal was Au. Roughness (rms) for Cu: 0.47 nm, and for Au: 1.12 nm.

Cu devices, the AFM results in Figure 5 imply that Au partially penetrates the NAB molecular layer while Cu does not (similar results were obtained for several different samples of PPF/NAB after removal of Cu or Au). Since both Raman and XPS data indicate that Au does not cause wide-spread structural damage to the NAB film, these results indicate that Au penetrates the molecular layer during deposition without widespread damage to the molecular structure. The surface energy for Cu is higher than that of Au,^[45] and we have reported previously that there is evidence from Raman and XPS that Cu interacts with the nitro group of NAB, while Au does not.^[46] It is possible that the lower enthalpy of interaction of Au with aromatic molecules is insufficient to compensate for the entropy increase associated with partial penetration of Au into the molecular layer. Thus, Cu appears to be the best choice for direct deposition of a top contact metal that will not disrupt the molecular layer.

2.4. Thermal Stability of Finished Device

In order to determine temperature window that a completed PPF/NAB/Cu device can withstand, we have subjected junctions to elevated temperatures in a vacuum environment. Figure 6 shows a series of J – V curves obtained after heat treatments of complete PPF/NAB/Cu devices. In each case, the sample was heated to the stated temperature for 5 min in vacuum, and then removed from the chamber and cooled to room temperature before testing. While there are no significant changes up to 190 °C, the conductance begins to increase at higher temperatures. After heating at 400 °C, the junction is ~ 33 times more conductive at 0.2 V. We reported recently that microfabricated carbon/NAB/Cu/Au junctions exhibited a slow conductance increase of 50% during 20 hours at 150 °C in vacuum, and were then stable for at least another 24 hours at 150 °C.^[34] Since a PPF/NAB sample without a top contact was shown to survive temperatures of 400 °C in the same vacuum environment (Figure 2), there are several possible explanations for

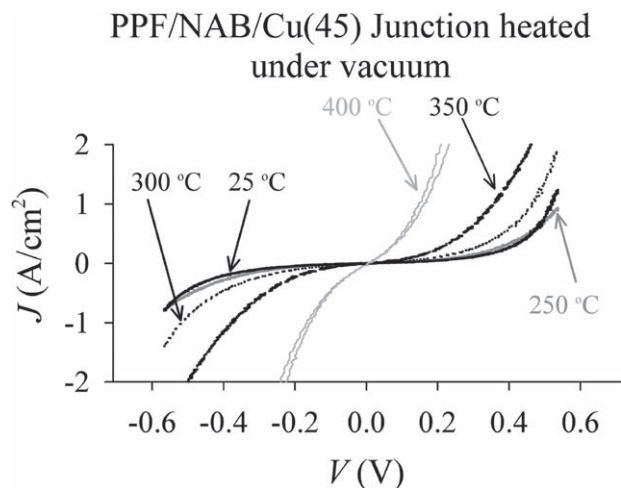


Figure 6. J - V curves of a single Si/SiO₂/PPF/NAB/Cu(45) junction heated in vacuum ($\sim 2 \times 10^{-6}$ torr) to progressively higher temperature for 5 min at each temperature. Samples were cooled in air before obtaining each J - V curve.

the increase in junction conductance after thermal treatments in the 200–400 °C range. First, annealing of the Cu top contact could reorder the Cu atoms, leading to an increase of the effective contact area of the junction.^[12] Second, a chemical reaction between the Cu and the NAB at elevated temperature could also alter junction conductance. Finally, although the molecular layer clearly is expected to remain intact (see Figure 2), penetration of Cu atoms due to their increased mobility at higher temperature is possible. In any case, it is clear that completed devices can survive temperature excursions to ~ 200 °C without large conductance changes, and that the molecular layer is stable beyond 400 °C. This level of temperature stability is significantly beyond that of most molecular electronics devices demonstrated to date.

2.5. Compatibility with Photolithography

Conventional photolithographic processing can involve harsh chemical treatments and significant UV radiation. Although this process is compatible with inorganic materials, the integration of “soft” organic molecules with lithographic processes is more challenging since many materials can undergo photo-degradation during the UV exposure,^[47–49] chemical reactions with resist components, and possible removal by solvents and developers. Recently we showed that a diazonium-derived molecular layer on titanium withstands sonication in acetone and acetonitrile, as well as 60 min in boiling water or 30 min in 0.1 M aqueous acid or base.^[40] In the current work, PPF/NAB samples were exposed to the photolithographic process of resist application/UV exposure/developing described in the Experimental Section. **Figure 7** shows Raman spectra for Si/SiO₂/PPF/NAB before and after a complete photolithographic process. The absence of changes in the spectrum for NAB indicates that this molecule is compatible with the photolithographic reagents and processing. In addition, diazonium-derived trifluoromethylphenyl (TFMP)

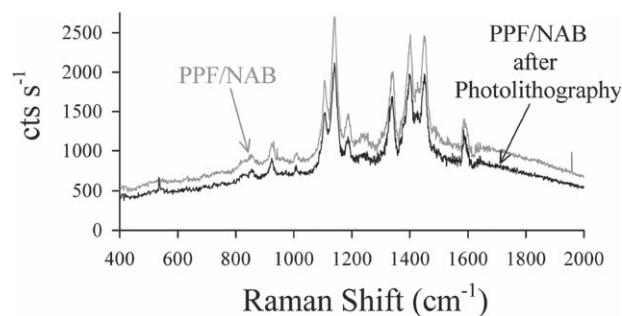


Figure 7. Raman Spectra of Si/SiO₂/PPF/NAB before (gray curve) and after (black curve) a complete photolithographic process (spin photoresist, UV exposure and development).

on PPF was also tested using XPS as a diagnostic and no change in the F/C ratio was observed after the photolithography process (see Figure S7 in the Supporting Information).

2.6. Sealing with parylene-N

Pyrolysis of the precursor di-*p*-xylylene at 600 °C under vacuum leads to dimer decomposition and production of gas-phase *p*-xylylene monomers. The *p*-xylylene monomers subsequently polymerize to parylene N (poly (*p*-xylylene)) on the sample surface, to produce a transparent hydrophobic film. The chamber maintains a sample temperature of ~ 30 °C.^[50] As such, parylene N has been used as protective layer for microelectronics applications due to its low gas and water permeability, high melting point,^[51] and hydrophobicity. In addition, it has good optical transparency^[51] and a low dielectric constant.^[52] **Figure 8A** shows J - V curves of a PPF/NAB(4.5)/Cu junction initially and after deposition of 0.3 μm parylene N. No significant changes in electronic behaviour occurred during parylene deposition, as expected, since the molecular junction is protected by the Cu top contact and the conditions during deposition are quite mild.

The effectiveness of parylene N as a barrier against moisture and chemical agents was investigated. The J - V curves shown in **Figure 8B** were obtained before and after immersion of a parylene-N coated PPF/NAB/Cu junction in 0.5 M FeCl₃ in water. Without the parylene coating, the FeCl₃ solution completely removed the Cu contact within 10 s, as described in section 2.3. As shown in **Figure 8B**, a 10 minute immersion in FeCl₃ had no effect on the electronic response of the parylene coated junction. The sample could also be immersed in water (**Figure S8** in supporting information) with the same result. These results indicate that parylene-N forms an excellent barrier to water and aqueous reagents, and that the molecular junctions are unaffected by parylene deposition.

3. Conclusions

Taken together, the results herein establish acceptable processing parameters for molecular electronic devices based on diazonium-modified carbon substrates. The strong carbon-carbon surface bond permits heating to at least

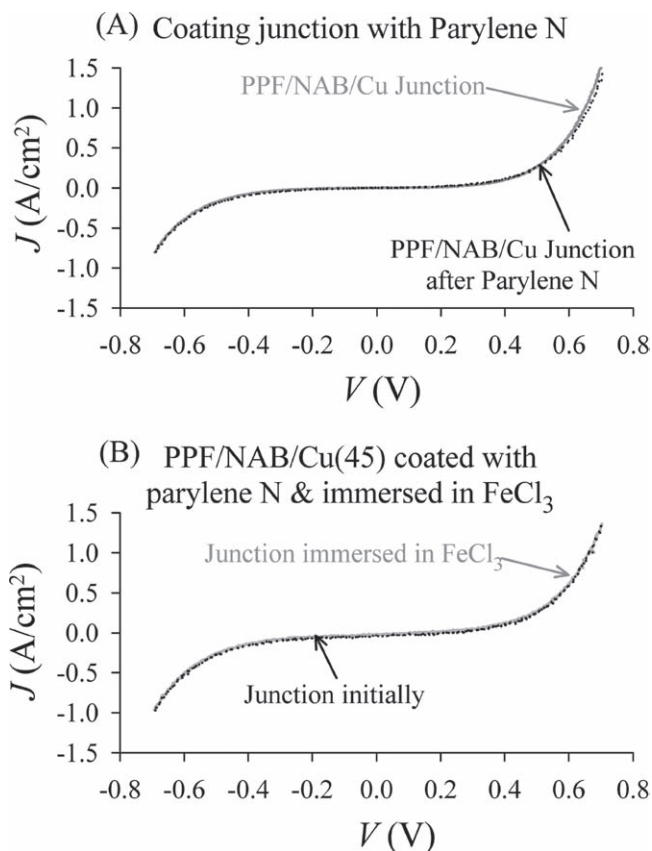


Figure 8. A) Electrical characterization of Si/SiO₂/PPF/NAB/Cu junction before and after encapsulation with 0.3 μm parylene N. B) *J*-*V* characteristic of parylene N coated Si/SiO₂/PPF/NAB-4/Cu junction and after immersion in 0.5 M FeCl₃ solution for 10 min.

400 °C in vacuum without breaking the surface-molecule covalent bond, or detectable perturbation of the molecular structure of NAB. In addition, irreversible bonding permits direct e-beam deposition of Cu and Au on diazonium-derived molecular layers without observable damage to the molecular structure, nor the formation of carbon/metal short circuits. Metal penetration has been a significant problem with Langmuir–Blodgett and Au/thiol monolayers, with direct vapour deposition often resulting in short circuits.^[19,20,22,24,53,54] Although these approaches benefit from ordering of molecules into a two-dimensional crystal, that ordering requires a labile molecule/surface bond in order to equilibrate to a low energy ordered state.^[4] Diazonium modification of carbon sacrifices some ordering to assure irreversible bonding to the surface^[4] and its associated thermal and chemical stability. Unlike Au and Cu, direct Ti and Pt deposition cause significant changes to the molecular layer, due to the reactivity of Ti and the high heat of condensation of Pt. The reproducibility of carbon/NAB/Cu devices was significantly better than carbon/NAB/Au, and the cause was revealed by AFM of the molecular layers after removing the metal by chemical etching. Cu had no observable effect on the surface of the molecular layer, while Au caused a significant increase in roughness, presumably caused by partial Au penetration into the film.

No observable changes in NAB layers derived from diazonium reduction on carbon were observed by XPS or Raman spectroscopy following exposure to FeCl₃, I₂/KI, or HF solutions in water, or from temperature excursions to 400 °C in vacuum. Finished devices could be heated to 250 °C without major changes in electronic properties, and sealing with parylene protected the devices from at least 10 min of exposure to water or FeCl₃ solution. PPF/NAB can be subjected to a complete resist/exposure/develop photolithography cycle with no apparent changes to the Raman spectrum, implying structural integrity throughout the process.

While there are many more requirements which must be met for integration of molecular devices with conventional microelectronics, the current work significantly extends the temperature range and acceptable processing steps. We demonstrated recently that the diazonium route to molecular junctions is compatible with microfabrication techniques, with high yield and good reproducibility.^[34] We are currently investigating the mechanism underlying increased conductance of completed devices at temperatures beyond ~250 °C, and also alternative electrode materials with higher thermal stability. These fabrication and device lifetime issues are being investigated in parallel with more fundamental studies of charge transport and electronic functions of molecular electronic devices.

4. Experimental Section

Acetonitrile, acetone, and isopropanol (HPLC grade, Fischer Scientific) were used as received. Water was purified by a Millipore system (18 MΩ, < 3 ppb TOC). 4-nitroazobenzene (NAB) 4'-diazonium tetrafluoroborate salt and 4-trifluoromethylphenyl (TFMP) diazonium tetrafluoroborate salt were prepared as described in detail elsewhere.^[55–57] Diced Si/SiO₂ chips (18 mm × 15 mm chips, 300 nm of thermally grown SiO₂) were used as substrates for all experiments except “back-side” Raman spectroscopy. In the later case, 25 mm × 25 mm × 0.22 mm quartz microscope cover slips (Technical Glass Products, Inc.) were used as an optically transparent support. Si/SiO₂ and Quartz (Q) substrates were cleaned by sonication in acetone, isopropanol and finally ultrapure water for 10 min each, and then dried in a directed stream of N₂. Pyrolyzed photoresist film (PPF) was prepared as outlined previously.^[12,58] Briefly, a positive photoresist (AZ P4330-RS, AZ Electronic Materials, Somerville, NJ) was spun onto clean substrates at 6000 rpm for 40 s (two coats) followed by soft baking at 90 °C for 15 min. The photoresist was then pyrolyzed by heating the samples in a tube furnace to 1025 °C (held for 60 min) under a constant flow of forming gas (5% H₂ in N₂ at 100 mL·min⁻¹). For XPS and AFM analysis, a blanket sheet of PPF was used. Optically transparent PPF (OTPPF) was prepared on quartz (Q) using diluted photoresist (5% v/v photoresist in propylene glycol methyl ether acetate as solvent).^[59,60] For junction fabrication, photoresist was patterned into 0.5 mm stripes using standard photolithography prior to pyrolysis.

Electrochemical modification of both PPF and Q/OTPPF with either NAB or TFMP diazonium salts were carried out using a 1 mM diazonium salt solution in acetonitrile with 0.1 M tetrabutylammonium tetrafluoroborate (TBABF₄) as the supporting electrolyte. Surface modification was carried out using four cyclic scans from +0.4 to -0.6 V versus Ag/Ag⁺ at a sweep rate of 0.2 V s⁻¹. We reported previously^[12] that this procedure yields an NAB film with a thickness of 4.5±0.3 nm, as determined with an AFM “scratching” technique,^[30] and the same NAB deposition conditions were used for all of the junctions reported herein. TFMP was bonded to PPF using the same procedure for XPS samples, but the molecular layer thickness was not determined. Following modification, PPF/NAB and Q/OTPPF/NAB samples were rinsed with acetonitrile and then dried in a directed stream of N₂. Modified PPF

substrates were then transferred to an electron-beam evaporator (Kurt J. Lesker PVD75), where various metals were deposited directly onto the surface of the molecular layer. For metals other than Ti, the chamber was evacuated to $\sim 2.2 \times 10^{-6}$ Torr before beginning deposition. For Ti, a lower pressure (2.2×10^{-7} Torr) was used to minimize its oxidation with residual gases in the chamber. For junction fabrication, metal was deposited through shadow mask (0.6 mm) oriented perpendicular to PPF strips to result in a cross-bar junction. The deposition rate was 3 \AA s^{-1} , except for Pt (0.1 \AA s^{-1}), and the metal thickness was measured by a quartz crystal microbalance (QCM). Junctions are designated from bottom to top with the metal layer thicknesses in nm in parentheses. For example, PPF/NAB/Cu(45) indicates a 4.5 nm NAB layer on 1–2 μm thick PPF with a Cu top contact 45 nm thick. In all cases where current-voltage behavior was determined, the junction area was $3.0 \times 10^{-3} \text{ cm}^2$.

Electrical characterization of molecular junctions utilized a three- or four-wire configuration^[12,25] where the top contact is virtual ground, with the drive voltage (V_{drive}) applied to PPF (thus, all voltages reported herein are indicate the voltage of the PPF relative to the top contact). The third and fourth probes are used to sense voltages on the PPF and top contact in order to compensate for ohmic losses (iR drop) due to the resistances of the leads. Data collection was done using a National Instruments 6111 or 6120 DAQ board controlled by Labview software to execute voltage sweeps and record the resulting current after amplification by an SRS 570 current amplifier.

Raman spectra were collected using a custom built spectrometer^[61] equipped with an Argon ion laser (514.5 nm), a 50 mm f/1.8 Nikon camera collection lens, a 2000 groove/mm holographic reflection grating, and a back scattering geometry that employs an Andor back-thinned charge-coupled device (CCD) detector cooled to -80° C .^[62] Incident power is $\sim 19 \text{ mW}$ and the signal is integrated for 30 s (unless stated otherwise). In order to perform characterization of NAB after metal deposition by XPS and AFM, the NAB molecular layer was exposed through wet chemical etching of the top metal. 0.5 M FeCl_3 , KI/I₂ solution (100g KI + 25g I₂ dissolved in 1L deionized H₂O), and 5% w/w HF were applied for a maximum of 10 s to etch Cu, Au, and Ti, respectively. The thermal stability of modified PPF was investigated by heating PPF/NAB in Ar gas or vacuum ($\sim 2 \times 10^{-6}$ torr) for 30 min (room temperature to 500°C) followed by Raman spectroscopy. Completed electronic junctions were heated under vacuum for 5 min (room temperature to 400 °C was tested) and then removed from vacuum and tested at room temperature.

To study the compatibility of modified PPF with photolithographic processes, a standard photoresist (HPR 504) was spun onto PPF/NAB and PPF/TFMP samples at 4000 rpm for 40 s, followed by UV exposure for 3 sec (365 nm and 404 nm, total intensity 65.3 mW cm^{-2}), and developer (Microposit 354). After developing, the sample was rinsed with deionized water and dried in a stream of N₂. Modified PPF samples were characterized by Raman and XPS before and after this procedure. Finally, encapsulation of completed devices with parylene was carried out. First, the junction was wired using silver epoxy so that the electrical properties could be probed before and after coating with 0.3 μm parylene N (PDS-2010 LABCOTER 2, Speciality Coating System). To ensure effective encapsulation, the electrical characterization was measured after immersing coated samples in water and 0.5 M FeCl_3 solution for 10 min.

Supporting Information

Figures and tables for several control and additional experiments are included in Supporting Information, including current-voltage curves, Raman spectra, and AFM images. Supporting Information is available from the Wiley Online Library or from the author.

Acknowledgements

This work was supported by NSERC, the National Institute for Nanotechnology, The University of Alberta, and the the MicroSystems

Technology Research Initiative. The National Institute for Nanotechnology is operated as a partnership between the National Research Council and the University of Alberta and is jointly funded by the Government of Canada, the Government of Alberta, and the University of Alberta. Portions of this work were carried out at the University of Alberta NanoFab facility. We also thank Dimitre Karpuzov at University of Alberta ACSES facility for collecting XPS spectra and intensity ratios, and Bryan Szeto for his help in thermal experiments and Jie Ru for providing an AFM scan for unmodified PPF.

Received: December 25, 2010

Published online: April 20, 2011

- [1] Semiconductor Industry Association, http://www.sia-online.org/cs/industry_resources/industry_fact_sheet. Accessed September, 2010
- [2] H. B. Akkerman, B. De Boer, *J. Phys.: Condensed Matter* **2008**, *20*, 013001.
- [3] R. L. McCreery, *Anal. Chem.* **2006**, *78*, 3490–3497.
- [4] R. L. McCreery, A. J. Bergren, *Adv. Mater.* **2009**, *21*, 4303–4322.
- [5] H. Haick, D. Cahen, *Acc. Chem. Res.* **2008**, *41*, 359–366.
- [6] A. Salomon, T. Boecking, O. Seitz, T. Markus, F. Amy, C. Chan, W. Zhao, D. Cahen, A. Kahn, *Adv. Mater.* **2007**, *19*, 445–450.
- [7] A. Salomon, D. Cahen, S. Lindsay, J. Tomfohr, V. B. Engelkes, C. D. Frisbie, *Adv. Mater.* **2003**, *15*, 1881–1890.
- [8] B. Ulgut, H. D. Abruna, *Chem. Rev.* **2008**, *108*, 2721–2736.
- [9] R. E. Holmlin, R. Haag, M. L. Chabynyc, R. F. Ismagilov, A. E. Cohen, A. Terfort, M. A. Rampi, G. M. Whitesides, *J. Am. Chem. Soc.* **2001**, *123*, 5075–5085.
- [10] F. Chen, J. Hihath, Z. F. Huang, X. L. Li, N. J. Tao, *Ann. Rev. Phys. Chem.* **2007**, *58*, 535–564.
- [11] P. A. Van Hal, E. C. P. Smits, T. C. T. Geuns, H. B. Akkerman, B. C. De Brito, S. Perissinotto, G. Lanzani, A. J. Kronemeijer, V. Geskin, J. Cornil, P. W. M. Blom, B. De Boer, D. M. De Leeuw, *Nature Nanotechnol.* **2008**, *3*, 749–754.
- [12] A. J. Bergren, K. D. Harris, F. J. Deng, R. L. McCreery, *J. Phys.: Condens. Matter* **2008**, *20*, 374117–374127.
- [13] L. Luo, C. D. Frisbie, *J. Am. Chem. Soc.* **2010**, *132*, 8854–8855.
- [14] E. A. Weiss, R. C. Chiechi, G. K. Kaufman, J. K. Kriebel, Z. F. Li, M. Duati, M. A. Rampi, G. M. Whitesides, *J. Am. Chem. Soc.* **2007**, *129*, 4336–4349.
- [15] F. Anariba, R. L. McCreery, *J. Phys. Chem. B* **2002**, *106*, 10355–10362.
- [16] C. Grave, E. Tran, P. Samori, G. M. Whitesides, M. A. Rampi, *Synth. Met.* **2004**, *147*, 11–18.
- [17] H. B. Akkerman, A. J. Kronemeijer, J. Harkema, P. A. van Hal, E. C. P. Smits, D. M. de Leeuw, P. W. M. Blom, *Org. Electron.* **2010**, *11*, 146–149.
- [18] M. Coll, C. A. Richter, C. A. Hacker, *J. Vac. Sci. Technol. B* **2009**, *27*, 2826–2831.
- [19] H. Haick, D. Cahen, *Acc. Chem. Research* **2008**, *41*, 359–366.
- [20] H. Haick, D. Cahen, *Prog. Surface Sci.* **2008**, *83*, 217–261.
- [21] Z. Zhu, D. L. Allara, N. Winograd, *Appl. Surface Sci.* **2006**, *252*, 6686–6688.
- [22] A. V. Walker, T. B. Tighe, O. M. Cabarcos, M. D. Reinard, B. C. Haynie, S. Uppili, N. Winograd, D. L. Allara, *J. Am. Chem. Soc.* **2004**, *126*, 3954–3963.
- [23] B. C. Haynie, A. V. Walker, T. B. Tighe, D. L. Allara, N. Winograd, *Appl. Surface Sci.* **2003**, *203*, 433–436.
- [24] G. L. Fisher, A. V. Walker, A. E. Hooper, T. B. Tighe, K. B. Bahnck, H. T. Skriba, M. D. Reinard, B. C. Haynie, R. L. Opila, N. Winograd, D. L. Allara, *J. Am. Chem. Soc.* **2002**, *124*, 5528–5541.
- [25] F. Anariba, J. K. Steach, R. L. McCreery, *J. Phys. Chem. B* **2005**, *109*, 11163–11172.

- [26] A. J. Bergren, R. L. McCreery, S. R. Stoyanov, S. Gusarov, A. Kovalenko, *J. Phys. Chem. C* **2010**, *114*, 15806–15815.
- [27] R. McCreery, *Chem. Mater.* **2004**, *16*, 4477–4496.
- [28] R. L. McCreery, *ChemPhysChem* **2009**, *10*, 2387–2391.
- [29] W. R. McGovern, F. Anariba, R. L. McCreery, *J. Electrochem. Soc.* **2005**, *152*, E176–E183.
- [30] F. Anariba, S. H. DuVall, R. L. McCreery, *Anal. Chem.* **2003**, *75*, 3837–3844.
- [31] J. K. Kariuki, M. T. McDermott, *Langmuir* **1999**, *15*, 6534–6540.
- [32] J. K. Kariuki, M. T. McDermott, *Langmuir* **2001**, *17*, 5947–5951.
- [33] R. L. McCreery, U. Viswanathan, R. P. Kalakodimi, A. M. Nowak, *Faraday Discuss.* **2006**, *131*, 33–43.
- [34] J. Ru, B. Szeto, A. Bonifas, R. L. McCreery *ACS Appl. Mater. Interfaces* **2010**, *2*, 3693–3701.
- [35] A. P. Bonifas, R. L. McCreery, *Nat. Nanotechnol.* **2010**, *5*, 612–617.
- [36] A. M. Nowak, R. L. McCreery, *Anal. Chem.* **2004**, *76*, 1089–1097.
- [37] A. M. Nowak, R. L. McCreery, *J. Am. Chem. Soc.* **2004**, *126*, 16621–16631.
- [38] E. Delonno, H. R. Tseng, D. D. Harvey, J. F. Stoddart, J. R. Heath, *J. Phys. Chem. B* **2006**, *110*, 7609–7612.
- [39] M. Toupin, D. Belanger, *J. Phys. Chem. C* **2007**, *111*, 5394–5401.
- [40] A. M. Mahmoud, A. J. Bergren, R. L. McCreery, *Anal. Chem.* **2009**, *81*, 6972–6980.
- [41] H. H. Liang, H. Tian, R. L. McCreery, *Appl. Spectrosc.* **2007**, *61*, 613–620.
- [42] T. Itoh, R. L. McCreery, *J. Am. Chem. Soc.* **2002**, *124*, 10894–10902.
- [43] P. S. Chen, *A new handbook of chemistry*; Chem. Elements Pub., Camarillo, CA **1975**.
- [44] C. H. deVilleneuve, J. Pinson, M. C. Bernard, P. Allongue, *J. Phys. Chem. B* **1997**, *101*, 2415–2420.
- [45] H. L. Skriver, N. M. Rosengaard, *Phys. Review B* **1992**, *46*, 7157.
- [46] R. L. McCreery, J. Wu, R. P. Kalakodimi, *Phys. Chem. Chem. Phys.* **2006**, *8*, 2572–2590.
- [47] J. Ficker, H. von Seggern, H. Rost, W. Fix, W. Clemens, I. McCulloch, *Appl. Phys. Lett.* **2004**, *85*, 1377–1379.
- [48] M. Manceau, J. Gaume, A. Rivaton, J. L. Gardette, G. Monier, L. Bideux, *Thin Solid Films* **2010**, *518*, 7113–7118.
- [49] T. Caronna, M. Forte, M. Catellani, S. V. Meille, *Chem. Mater.* **1997**, *9*, 991–995.
- [50] P. Kramer, A. K. Sharma, E. E. Hennecke, H. Yasuda, *J. Polym. Sci., Part A* **1984**, *22*, 475–491.
- [51] Y. S. Yeh, W. J. James, H. Yasuda, *J. Polym. Sci., Part B* **1990**, *28*, 545–568.
- [52] J. J. Senkevich, S. B. Desu, *Appl. Phys. Lett.* **1998**, *72*, 258–260.
- [53] R. M. Metzger, *Acc. Chem. Res.* **1999**, *32*, 950.
- [54] R. M. Metzger, T. Xu, I. R. Peterson, *J. Phys. Chem. B* **2001**, *105*, 7280–7290.
- [55] H. H. Yang, R. L. McCreery, *J. Electrochem. Soc.* **2000**, *147*, 3420–3428.
- [56] S. H. DuVall, R. L. McCreery, *J. Am. Chem. Soc.* **2000**, *122*, 6759–6764.
- [57] P. Allongue, M. Delamar, B. Desbat, O. Fagebaume, R. Hitmi, J. Pinson, J. M. Saveant, *J. Am. Chem. Soc.* **1997**, *119*, 201–207.
- [58] S. Ranganathan, R. McCreery, S. M. Majji, M. Madou, *J. Electrochem. Soc.* **2000**, *147*, 277–282.
- [59] S. Donner, H. W. Li, E. S. Yeung, M. D. Porter, *Anal. Chem.* **2006**, *78*, 2816–2822.
- [60] H. Tian, A. J. Bergren, R. L. McCreery, *Appl. Spectrosc.* **2007**, *61*, 1246–1253.
- [61] J. D. Ramsey, S. Ranganathan, J. Zhao, R. L. McCreery, *Appl. Spectrosc.* **2001**, *55*, 767–773.
- [62] L. C. T. Shoute, A. J. Bergren, A. M. Mahmoud, K. D. Harris, R. L. McCreery, *Appl. Spectrosc.* **2009**, *63*, 133–140.